

## One THz harmonic oscillation of resonant tunneling diodes

N. Orihashi and S. Suzuki

*Interdisciplinary Graduate School of Science and Engineering, Tokyo Institute of Technology, 2-12-1-S9-3 O-okayama, Meguro-Ku, Tokyo 152-8552, Japan*

M. Asada<sup>a)</sup>

*Interdisciplinary Graduate School of Science and Engineering, Tokyo Institute of Technology, CREST, Japan Science and Technology Agency, 2-12-1-S9-3 O-okayama, Meguro-Ku, Tokyo 152-8552, Japan*

(Received 8 July 2005; accepted 7 October 2005; published online 29 November 2005)

One THz harmonic oscillation was observed in a sub-THz oscillating GaInAs/AlAs resonant tunneling diode integrated with a slot antenna. The fundamental and third-harmonic frequencies were 342 GHz and 1.02 THz, respectively, for a 50  $\mu\text{m}$  long antenna. The maximum output power of the fundamental mode was around 23  $\mu\text{W}$ , and that of the third-harmonic component was 2.6% of the fundamental. Theoretical analysis with the van der Pole equation qualitatively explained the measured results. © 2005 American Institute of Physics. [DOI: 10.1063/1.2139850]

The terahertz (THz) frequency range is receiving considerable attention recently because of its many possible applications, such as in imaging, spectroscopy in chemistry and biotechnology, and high-capacity communications. For these applications, compact and coherent solid-state light sources are important key components. For semiconductor devices, quantum cascade lasers<sup>1,2</sup> and *p*-Ge lasers<sup>3</sup> oscillating in the THz range have been reported. Electron devices toward the THz range are also being developed from the low-frequency side.<sup>4–11</sup> Resonant tunneling diodes (RTDs) have been considered as one of the candidates for the THz oscillators at room temperature.<sup>4–7</sup>

Oscillation of harmonic frequency in single devices is also investigated in IMPATT, Gunn, and TUNNETT diodes<sup>11–15</sup> and superlattices,<sup>16</sup> as well as frequency multipliers using external low-frequency sources. In this letter, harmonic oscillation of 1 THz is reported for RTDs oscillating in sub-THz range at room temperature. To our knowledge, this is the highest frequency to date from a room-temperature single semiconductor electronic oscillator, although it is a harmonic component.

The structure of the fabricated RTD oscillator is shown in Fig. 1. An InGaAs-AlAs double-barrier RTD with the area of  $2 \times 2 \mu\text{m}^2$  is located at the center of a slot antenna. The layer structure of the RTD is, from the top,  $n^+$ -GaInAs ( $10^{18}$ – $10^{19} \text{ cm}^{-3}$ , 30 nm)/*n*-GaInAs ( $10^{17} \text{ cm}^{-3}$ , 50 nm)/GaInAs (undoped, 5 nm)/barrier AlAs (undoped, 5 monolayers)/well GaInAs (undoped, 4.5 nm)/barrier AlAs (undoped, 5 monolayers)/GaInAs (undoped, 5 nm)/*n*-GaInAs ( $10^{17} \text{ cm}^{-3}$ , 50 nm)/ $n^+$ -GaInAs ( $10^{18}$ – $10^{19} \text{ cm}^{-3}$ , 400 nm) on a semi-insulating InP substrate. The GaInAs layers are lattice-matched to InP.

The left and right electrodes of the slot antenna are connected to the upper and lower sides of the RTD, respectively. At both ends of the slot, these electrodes are overlapped with a 100 nm-thick  $\text{SiO}_2$  inserted between them. By this metal/insulator/metal (MIM) structure, high frequency electromagnetic waves are reflected at both ends of the slot, and a standing wave is formed. The bridging lead between the upper

side of the RTD and the antenna electrode is 6  $\mu\text{m}$  wide and 4  $\mu\text{m}$  long, and is designed to be slightly larger than the RTD to act as a heat sink. The antenna electrode is Au/Pd/Ti with the thicknesses of 750/20/20 nm for the left part and 70/15/10 nm on 400 nm-thick  $n^+$ -GaInAs layer for the right part. A sheet resistor of bismuth is deposited parallel to the RTD on the outside of the antenna to suppress low-frequency (2 to 3 GHz) parasitic oscillations originating from the resonance with the external bias circuits.

In the fabrication process, an approximately 500  $\mu\text{m} \times 1 \text{ mm}$  and 700 nm high mesa of the RTD layer was first formed by electron-beam (EB) lithography for the foundation of the right-hand-side electrode of the slot antenna in Fig. 1, by a serial process consisting of the deposition of Ti/Au/Ti for etching mask,  $\text{CH}_4$  and  $\text{H}_2$  reactive ion etching (RIE) and wet chemical etching ( $\text{H}_2\text{O}:\text{H}_2\text{SO}_4:\text{H}_2\text{O}_2 = 40:1:1$ ). In order to avoid contact of the left-hand-side electrode with the side wall of the RTD mesa, the foundation of the right-hand-side electrode was coated by benzo-cyclobutene (BCB). After etching BCB by RIE ( $\text{CF}_4$  and  $\text{O}_2$ ), the top Ti/Au/Ti was removed with HF. The un-overlapped part of the left-hand-side electrode and the bridging lead between the RTD and the left-hand-side electrode was fabricated by EB lithography and Au/Pd/Ti deposition. The RTD rectangular mesa with the area of around  $4 \mu\text{m}^2$  was fabricated by

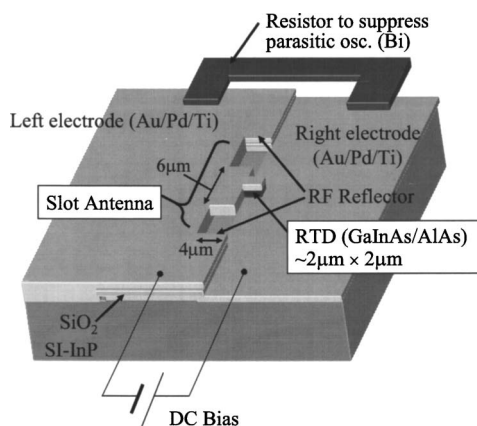


FIG. 1. Fabricated structure of RTD oscillator integrated with slot antenna.

<sup>a)</sup>Electronic mail: asada@pe.titech.ac.jp

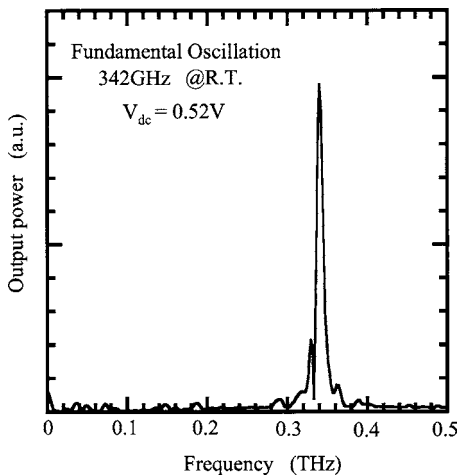


FIG. 2. Measured spectrum of fundamental oscillation for the device with 50  $\mu\text{m}$  long antenna.

RIE ( $\text{CH}_4$  and  $\text{H}_2$ ) and wet chemical etching of the foundation of the right-hand-side electrode. Then, the right-hand-side electrode was fabricated by EB lithography and Au/Pd/Ti deposition. The upper electrode of the MIM reflector was finally fabricated by  $\text{SiO}_2$  plasma chemical vapor deposition, EB lithography, deposition of Au/Cr, RIE ( $\text{CF}_4$  and  $\text{O}_2$ ) for  $\text{SiO}_2$  etching, and deposition of Au/Cr for connection to the left-hand-side electrode.

The peak current density of the fabricated RTD was typically around 300  $\text{kA}/\text{cm}^2$ , and the peak-to-valley current ratio was around 2. Output power was measured from the bottom of the substrate through a hemispherical Si lens and an off-axis paraboloidal mirror with a He-cooled Si composite bolometer. Oscillation spectra were measured with a Fourier transformed infrared spectrometer. In the measurement of harmonic oscillations, a high-pass mesh filter with the cut-off frequency of 600 GHz ( $>$  fundamental frequency of the measured samples) was inserted to avoid mixing with the spurious harmonics from the fundamental component in the Fourier transformation. Measurements were performed under pulsed current conditions by the lock-in technique to eliminate surrounding noise from the detector. The pulse duration was 0.3 ms and the repetition frequency was 300 Hz. For the fundamental mode oscillation, measurement under continuous current was also carried out, and the output power was found to be almost the same as that obtained under the pulsed condition.

Figure 2 shows the measured spectrum of the fundamental oscillation of the device with a 50  $\mu\text{m}$  long antenna. The negative differential resistance (NDR) region was 0.37–0.65 V, and the bias voltage in Fig. 2 was 0.52 V. The maximum output power was obtained in the range of 0.5–0.55 V, and was estimated to be 23  $\mu\text{W}$ . The fundamental frequency was 342 GHz at the maximum output power. Figure 3 shows the measured spectra of the harmonic components for various bias voltages after eliminating the fundamental component with the high-pass filter. Since the fundamental frequency increases slightly with bias voltage,<sup>7</sup> the harmonic frequencies also change in the same manner. The frequency of the third harmonic component was 1.02 THz at 0.55 V. The output powers of the harmonic components depend on bias voltage, as shown in Fig. 3. Near the center of the NDR region [Fig. 3(b)], the second harmonic vanishes. This agrees qualitatively with the theoretical

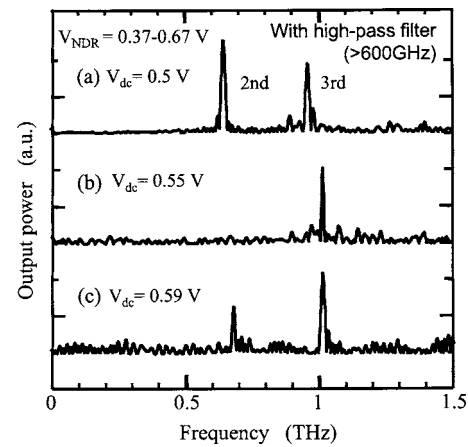


FIG. 3. Measured spectra of the second and third harmonics with high-pass filter ( $>600$  GHz) cutting of the fundamental mode for the device with 50  $\mu\text{m}$  long antenna for various bias voltages.

analysis shown below. The output power was 2.6% (0.59  $\mu\text{W}$ ) of the fundamental component for the third harmonics at 0.55 V.

The harmonic components included in the oscillation was calculated theoretically with the simple equivalent circuit shown in the inset of Fig. 4, where  $v(t)$  is the oscillation voltage,  $-G_d$  is the differential conductance of the RTD,  $L$  and  $C$  are the equivalent inductance and capacitance of the antenna resonator, and  $G_L$  is the load conductance of the antenna. The parasitic elements are neglected for simplicity, because the main conclusions are not changed.  $-G_d$  is assumed to depend on bias voltage as<sup>17</sup>  $-G_d = -a + 3b(v + V_0)^2$ , where  $a$  and  $b$  are constants, and  $V_0$  is the bias voltage measured from the center of the NDR region. The oscillation voltage across the RTD is obtained from the following van der Pole equation

$$\frac{d^2\xi}{d\tau^2} - \varepsilon[1 - (\xi + \xi_0)^2]\frac{d\xi}{d\tau} + \xi = 0, \quad (1)$$

where  $\tau = \omega_0 t$  with  $\omega_0 = 1/\sqrt{LC}$ ,  $\xi = \sqrt{3b/(a - G_L)}v$ ,  $\xi_0 = \sqrt{3b/(a - G_L)}V_0$ , and  $\varepsilon = (a - G_L)/\omega_0 C$ . The NDR region is

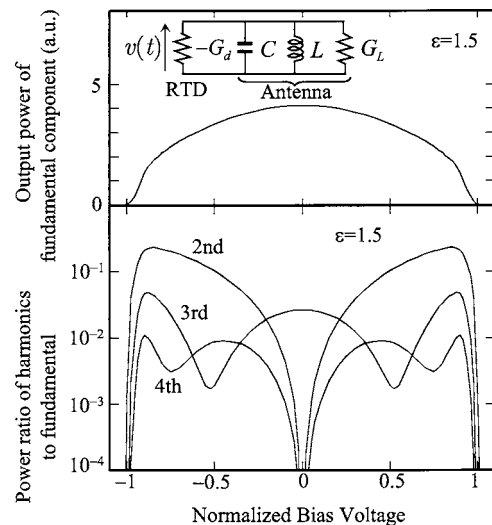


FIG. 4. Calculated results of fundamental output power and power ratios of the harmonics, as a function of normalized bias voltage in which the origin is shifted to the center of the NDR region.

$|\xi_0| \leq \sqrt{a/(a-G_L)}$ , and the oscillation is possible in the bias range of  $|\xi_0| \leq 1$ . The voltage amplitudes of the harmonics were obtained from the Fourier expansion coefficients of the numerical solution of Eq. (1) after many periods of oscillation. The output power is proportional to the absolute square of the Fourier expansion coefficient for each harmonic component.

Figure 4 shows the calculated results of the fundamental output power and the power ratios of the harmonics to the fundamental, as a function of normalized bias voltage  $\xi_0$  for  $\varepsilon=1.5$ . At the center of the NDR region ( $\xi_0=0$ ), the second and fourth components vanish, because  $-G_d$  is symmetric with respect to  $v(t)$  at this point. In spite of the simplified model, the central part of Fig. 4 qualitatively explains the behavior of the harmonic components in Fig. 3.  $V_{dc}=0.5, 0.55$  and  $0.59$  V in Fig. 3 correspond to  $\xi_0=-0.9, 0$  and  $0.8$ , respectively. In the region away from the NDR, the theoretical output power of the 4th harmonic is not negligible compared with the third harmonic. However, the fourth harmonic was not observed in the experiment in the whole range of the fundamental oscillation. Exact calculation may be possible with a precise dependence of  $-G_d$  on bias voltage and the inclusion of parasitic elements.

Harmonic components increase with increasing  $\varepsilon$  in Eq. (1). A large  $\varepsilon$  can be achieved by reducing  $C$  or increasing  $a$ . The theoretical ratio of the third harmonic to the fundamental components increases from 2.7% to 3.9% at the center of the NDR region, when  $\varepsilon$  increases from 1.5 to 2. The addition of resonance circuits for harmonic components may also be effective. However, the fundamental oscillation over 1 THz is the most important and effective for THz single oscillators with high output power, which is theoretically possible by reducing the size of the slot antenna.<sup>6</sup> We believe the experimental results presented in this letter imply that RTDs can also operate over 1 THz in the fundamental oscillation mode.

In conclusion, 1 THz harmonic oscillation was observed in sub-THz oscillating GaInAs/AlAs resonant tunneling diode integrated with a slot antenna. The fundamental and third harmonic frequencies were 342 GHz and 1.02 THz, respectively, for a 50  $\mu\text{m}$ -long antenna. The output power of the fundamental mode was around 23  $\mu\text{W}$ , and the third harmonic component was 2.6% of the fundamental. Theoretical

results of the van der Pole equation reasonably agreed with the measured results.

The authors acknowledge emeritus Professor Y. Suematsu of the Tokyo Institute of Technology for continuous encouragement. The authors also acknowledge Professor K. Furuya and Professor S. Arai, and Associate Professor Y. Miyamoto and Associate Professor M. Watanabe for fruitful discussions. This work was supported by the Ministry of Education, Culture, Sports, Science and Technology, by the Ministry of Public Management, Home Affairs, Posts and Telecommunications and by the International Communications Foundation.

- <sup>1</sup>R. Köhler, A. Tredicucci, F. Beltram, H. E. Beere, E. H. Linfeld, A. G. Davies, D. A. Ritchie, R. C. Iotti, and F. Rossi, *Nature (London)* **417**, 156 (2002).
- <sup>2</sup>B. S. Williams, S. Kumar, Q. Hu, and J. L. Reno, *Electron. Lett.* **40**, 431 (2004).
- <sup>3</sup>S. Komiyama, *Phys. Rev. Lett.* **48**, 271 (1982).
- <sup>4</sup>E. R. Brown, J. R. Sönderström, C. D. Parker, L. J. Mahoney, K. M. Molvar, and T. C. McGill, *Appl. Phys. Lett.* **58**, 2291 (1991).
- <sup>5</sup>M. Reddy, S. C. Martin, A. C. Molnar, R. E. Muller, R. P. Smith, P. H. Siegel, M. J. Mondry, M. J. W. Rodwell, H. Kroemer, and S. J. Allen, *IEEE Electron Device Lett.* **58**, 218 (1997).
- <sup>6</sup>N. Orihashi, S. Hattori, and M. Asada, *Int. Conf. on Infrared and Millimeter Waves, M5.3*, Karlsruhe/Germany, Sept. 2004.
- <sup>7</sup>N. Orihashi, S. Hattori, S. Suzuki, and M. Asada, *Electron. Lett.* **41**, 872 (2005).
- <sup>8</sup>M. J. W. Rodwell, M. Urteaga, Y. Betsler, T. Mathew, P. Krishnan, D. Scott, S. Jaganathan, D. Mensa, J. Guthrie, R. Pallela, Q. Lee, B. Agarwal, U. Bhattachaya, and S. Long, *Int. J. High Speed Electron. Syst.* **11**, 159 (2001).
- <sup>9</sup>W. Hafez and M. Feng, *Appl. Phys. Lett.* **86**, 152101 (2005).
- <sup>10</sup>Y. Yamashita, A. Endoh, K. Shinohara, K. Hikosaka, T. Matsui, S. Hiyamizu, and T. Mimura, *IEEE Electron Device Lett.* **23**, 573 (2003).
- <sup>11</sup>P. Plotka, J. Nishizawa, T. Kurobayashi, and H. Makabe, *IEEE Trans. Electron Devices* **50**, 867 (2003).
- <sup>12</sup>M. Ohmori, T. Ishibashi, and S. Ono, *IEEE Trans. Electron Devices* **ED-24**, 1323 (1977).
- <sup>13</sup>H. Barth and W. Menzel, *IEEE MTT-S Int. Microwave Symp. Dig.* **O-2**, 367 (1985).
- <sup>14</sup>A. Rydberg, *IEEE Electron Device Lett.* **11**, 439 (1990).
- <sup>15</sup>H. Eisele, M. Naftaly, R. Kamoua, *Int. J. Infrared Millim. Waves* **26**, 1 (2005).
- <sup>16</sup>E. Shomburg, J. Grenzer, K. Hofbeck, T. Blomeier, S. Winnerl, S. Brandl, A. A. Ignatov, K. F. Renk, D. G. Pavel'ev, Yu. Koschurinov, V. Ustinov, A. Zhukov, A. Kovsch, S. Ivanov, and P. S. Kop'ev, *Solid-State Electron.* **42**, 1495 (1998).
- <sup>17</sup>C. S. Kim and A. Brändli, *IRE Trans. Circuit Theory* **CT-8**, 416 (1961).